Microporous and Mesoporous Materials 302 (2020) 110202

Contents lists available at ScienceDirect

Microporous and Mesoporous Materials

journal homepage: http://www.elsevier.com/locate/micromeso

Silicalite-1 synthesized with geothermal and Ludox colloidal silica and corresponding TiO_2/silicalite-1 hybrid photocatalysts for VOC oxidation

Silvia Suárez [a,*], Roxana Postolache [b], F. Javier García-García [c], Benigno Sánchez [a], Roger Rothon [b], Aidan M. Doyle [b], Lubomira Tosheva [b,*]

[a] FOTOAir-Ciemat, Unit of Analysis and Photocatalytic Treatment of Pollutants in Air, Avda. Complutense 40, 28040, Madrid, Spain
[b] Department of Natural Sciences, Manchester Metropolitan University, Chester St., Manchester, M1 5GD, United Kingdom
[c] ICTS-CNM, Universidad Complutense de Madrid, 28040, Madrid, Spain

ARTICLE INFO

Keywords:
Photocatalysis
VOCs
Air treatment
Geothermal silica
Zeolite/TiO_2 hybrids

ABSTRACT

Silicalite-1 samples of uniform sub-micron size with two distinct morphologies were prepared using colloidal silica extracted from geothermal fluids. The colloidal silica used was provided by a New Zealand Company, GEO40 Ltd, and was produced by them using their patented process for recovering colloidal silica from geothermal brine. Spherical crystals with an average size of ca. 250 nm (S1N) as well as typical MFI-type coffin-shaped crystals with a size of ca. 900 nm (S1M) were prepared from clear synthesis solutions made from colloidal silica and aqueous tetrapropylammonium hydroxide of different concentration. The silicalite-1 samples prepared showed very similar characteristics to samples prepared using a conventional silica sol, Ludox SM, as a silica source. Silicalite-1 samples prepared with geothermal and conventional silica sols were used as supports for TiO_2 nanoparticles. The hybrid TiO_2/silicalite-1 materials were tested as photocatalysts for the photocatalytic degradation of trichloroethylene for air pollution control. The hybrid samples reduced the formation rates of non-desirable reaction products, promoting the mineralization process in comparison with a reference TiO_2 xerogel and high Si/Al ratio ZSM-5-based hybrid materials.

1. Introduction

Growing water and air pollution with a plethora of pollutants specific for different parts of the world requires urgent attention. The development of clean technologies, which are applicable to non-selective treatment of contaminants in solution and in the gas phase and capable of degrading the pollutants into benign products, is of upmost importance. Heterogeneous photocatalysis based on the use of TiO_2 nanopowders have been considered as a promising approach [1–5]. Drawbacks associated with the use of TiO_2 fine particles include recovery issues from solution, low adsorption capacity and fast electron/hole recombination. Adsorption-photocatalyst hybrids (APH) based on porous adsorbents and a semiconductor, e.g., TiO_2, have demonstrated improved photocatalytic performance because of synergy between the high surface area porous adsorbent and the photocatalyst [6,7]. Amongst different adsorbents, zeolites have shown promising potential as support materials for TiO_2. Zeolite/TiO_2 composite materials with TiO_2 content of up to 50 wt% have been prepared by methods such as sol-gel and impregnation [8–19]. A relatively small number of zeolite types have been used as supports, namely ZSM-5 [8–15], Y [11–17], beta [12–14], mordenite [11,16,17] and natural zeolites [18,19]. Different pollutants have been used in these studies, which often makes it difficult to draw conclusions about the influence of the zeolite type on the performance of zeolite-supported photocatalysts. Hydrophobicity has been found to have a positive effect on the photocatalytic activity, by either increasing the adsorption capacity for organic compounds [14] or by increasing the accessibility of the active TiO_2 sites [15]. Furthermore, zeolites have been shown to delay recombination rates of electron/hole pairs [16], suppress the formation of non-desirable reaction products [10], minimize detrimental effects of coexisting substances [20] and facilitate complete mineralization [14]. For example, TiO_2/ZSM-5 hybrids synthesized with a ZSM-5 of high Si/Al ratio, reduced the formation of toxic by-products [12]. High TiO_2 dispersion on the zeolite surface and the intimate contact between both phases lead to a synergistic effect, as was demonstrated by changing the adsorbent-photocatalyst configuration in the photoreactor [10]. Zeolite/TiO_2 hybrids have also been found to be superior to bare TiO_2 in

* Corresponding authors.
E-mail addresses: silvia.suarez@ciemat.es (S. Suárez), l.tosheva@mmu.ac.uk (L. Tosheva).

https://doi.org/10.1016/j.micromeso.2020.110202
Received 14 November 2019; Received in revised form 21 February 2020; Accepted 23 March 2020
Available online 8 April 2020

real-life systems, such as wastewaters from the textile industry and aquaculture wastewaters [16,20]. Liu et al. have demonstrated the possibility to regenerate TiO_2/zeolites adsorbents via exposure to UV irradiation following pollutant adsorption [21]. Simple mechanical mixing of TiO_2 with silicalite-1 has been found to completely decompose 2-propanol in air while eliminating intermediate molecules [22]. This work suggests silicalite-1 as a potential candidate for preparation of TiO_2/-zeolite hybrids. Moreover, the photoefficiency of these materials towards more complex molecules such us organochloride compounds instead of dyes, and under harsher operating conditions, should be explored. A single pass photoreactor working at low residence time would allow the determination of the performance of these materials under real conditions.

Nanozeolites have attracted much attention because of their potential to overcome drawbacks of conventional zeolites such as diffusion limitations, their use for preparation of zeolite membranes and as model systems for zeolite crystallization mechanism studies [23]. Owing to its aluminum-free composition and highly reproducible synthesis, silicalite-1 prepared from tetraethoxysilane (TEOS) and aqueous tetrapropylammonium hydroxide (TPAOH) is one of the most studied nanozeolite systems [24]. The abundant use of TPAOH in this system and associated cost and waste issues have led to the development of strategies aimed at minimizing the amount of template used, for instance via seed-induced crystallization [25]. Efforts have also been focused on increasing the yield of nanosized silicalite-1 by introducing additional synthetic steps and high temperature treatment [26,27]. The replacement of TEOS with cheaper amorphous silica sources such as colloidal silica has also been explored [28,29]. Compared to TEOS, synthesis of silicalite-1 in the presence of colloidal silica (Ludox) results in more complex nucleation processes, longer crystallization times, larger crystal sizes and broader particle size distributions. Amorphous silica extracted from waste materials such as fly ash and rice husks has been employed for the synthesis of MFI-type nanozeolites as well [30,31]. Silica is a major component of geothermal fluids, causing scaling and waste concerns to geothermal facilities [32]. Silica scaling is a significant issue and cost to manage in the generation of renewable geothermal energy. The removal of the silica can also allow the geothermal power generator to generate more renewable power from the water. The transformation of this silica to a useful product i.e. zeolite based catalyst, would be an advancement on the present system.

Most of the studies above deal with TiO_2/zeolite hybrids prepared using commercial zeolites. However, the influence of the morphology and size of the zeolite crystals has not been considered. To the best of our knowledge, nanozeolites have not been used as supports for TiO_2 for photocatalytic applications so far. In this work, silica extracted from geothermal reinjection fluids was used for the synthesis of nanosized silicalite-1 and the results were compared to silicalite-1 prepared with a conventional silica sol. Nanosized silicalite-1 of two different morphologies were prepared and used as supports for TiO_2 nanoparticles. The photocatalytic activity of the hybrid samples was studied for the degradation of trichloroethylene in the gas phase under low power UV-A lamps. Trichloroethylene is a very toxic organochloride compound, which is used in large quantities as solvent. Exposure to trichloroethylene has been linked to an increased cancer risk, which is the reason for selecting this compound as model VOC in this study [33].

2. Experimental

2.1. Synthesis of silicalite-1

The colloidal silica (GEO40™ SOL-1030Na) used for the synthesis of silicalite-1 was provided by a New Zealand Company, GEO40 Ltd, and was produced by them using their patented process for recovering colloidal silica from geothermal brine. It was obtained as a 30 wt% suspension in water stabilized by sodium hydroxide. Silicalite-1 was prepared from clear solutions containing GEO40™ SOL-1030Na, tetrapropylammonium hydroxide (TPAOH, 1 M aqueous solution, Alfa Aesar) and distilled water. Two molar compositions were used, namely $25SiO_2$: 9TPAOH: $595H_2O$ and $25SiO_2$: 3TPAOH: $1494H_2O$, and corresponding samples prepared were labelled as GS1N and GS1M, respectively. The solutions were prepared by mixing the components of the precursor mixture in a beaker (no additional water was added for the synthesis of GS1N), and stirring for 1 h. The mixtures were then transferred to 500 mL polypropylene reactors and hydrothermally treated at 90 °C for 2 d (GS1N) or 5d (GS1M). After the synthesis, the samples were purified by three-times centrifugation (6000 rpm) and redispersion in distilled water and dried at 90 °C overnight. The TPA template was removed by calcination at 500 °C for 5 h after heating to this temperature at a heating rate of 10 °C min^{-1}. Samples were prepared analogously using commercial Ludox SM colloidal silica (30 wt% suspension in water, Aldrich). These samples were labelled as LS1N and LS1M, respectively.

2.2. Preparation of TiO_2/silicalite-1 hybrids

TiO_2 nanoparticles were immobilized onto the silicalite-1 microporous materials by incipient wetness impregnation. A TiO_2 sol was synthesized as described elsewhere [34]. A TiO_2-sol volume equal to the total pore volume of silicalite-1 samples was added to the microporous materials. The TiO_2 loading of the final composites was set to 8 wt%, according to previous studies [12]. Moreover, for characterization purposes, TiO_2 xerogel was obtained by drying the TiO_2 sol at room temperature. Then, the material was thermally treated at 500 °C for 3 h. Hybrid TiO_2/silicalite-1 photocatalysts were labelled as AS1B-Ti, where A is G or L depending on the silica sol used, Geosol or Ludox, correspondingly, and B is N or M depending on the molar composition of the synthesis solution (GS1N-Ti, GS1M-Ti, LS1N-Ti and LS1M-Ti).

2.3. Characterization techniques

The morphology of the silicalite-1 samples was studied by scanning electron microscopy (SEM) using a Carl Zeiss Ltd Supra 40VP Scanning Electron Microscope. X-ray diffraction (XRD) patterns were measured with an X'Pert PANalytical X-ray diffractometer, employing Cu Kα radiation (40 kV and 30 mA) and a PIXcell detector. Nitrogen adsorption-desorption isotherms were collected at −196 °C with a Micromeritics ASAP2020 instrument. Calcined samples were degassed at 300 °C overnight prior to analysis. Surface areas S_{BET} were calculated using the BET equation and pore-size distributions were determined by the BJH method from the desorption branches of the isotherms. Micropore volumes V_μ were determined by the t-plot method. Particle size distributions were measured by dynamic light scattering (DLS) using a Zetasizer Nano ZS instrument with a 173° backscattering angle geometry. Raman spectra of the hybrid materials were measured with a ThermoScientific DXR Raman microscope equipped with a 532 nm laser using a power of 10 mW, an exposure time of 2 s and averaging 20 exposures.

High-resolution transmission electron microscopy (HRTEM, JEOL 2100HT) operated at 200 kV, was used to examine the particle size and dispersion of TiO_2 into the zeolites as well as to obtain structural information of the materials. Specimens for electron microscopy were prepared by dispersing the samples in butanol in an ultrasound bath. A few droplets of the resulting dispersion were put onto copper grids coated with a holey amorphous carbon thin layer for TEM. The isoelectric points (IEPs) were estimated by microeelectrophoresis laser Doppler, analyzing the changes of the zeta potential with the pH using a Malvern Zetasizer Nano ZS90 with MPT-2 autotitrator. Experiments were carried out using 15 mg of power sample suspended in 100 mL of 10^{-3} M KCl solutions, adjusting the pH values with 0.25 M and 0.025 M HCl or KOH solutions. The measurements were repeated three times to ensure reproducibility. The isoelectric point (IEP) of the samples were calculated using Henry's law with Smoluchowski's approximation [35]. The modified Park's equation was used to calculate the apparent molar

fraction of exposed TiO_2 [36].

2.4. Photocatalytic measurements

The photocatalytic activity experiments were evaluated in a continuous-flow flat reactor, at different total gas flows between 500 and 900 mL min^{-1} and residence times, *tr*, between 0.78 and 0.43 s. A stainless steel reactor with external dimensions of 120 mm × 50 mm × 10 mm (length × width × depth) was covered with a borosilicate glass window of 37 cm^2. 30 mg of material was placed on a borosilicate glass slide (70 mm × 26 mm) and was introduced in the photoreactor. Gas cylinders (Air Liquide) with controlled compositions of C_2HCl_3/N_2 (250 ppm) were used to obtain the desired concentration of pollutant in the reactor inlet by means of mass flow controllers (MFC). Experiments were performed with inlet concentrations of trichloroethylene (C_2HCl_3) of 25 ppm in CO_2 and moisture-free air. Two UV-A lamps (8 W Philips and 6.5 mW cm^{-2} irradiance) were used as the irradiation source. The oxygen content in the gas flow ranged between 15 and 20% in all experiments. The gas composition at the reactor inlet and outlet was analyzed with FTIR spectroscopy using a Thermo-Nicolet 5700 spectrometer equipped with a gas cell at 110 °C. The evolution of reactants and reaction products during the photocatalytic reaction was monitored by following the characteristic vibrational bands of the desired molecules. Before each experiment, and in order to eliminate impurities, each sample was irradiated with UV-A lamps for 12 h under air atmosphere.

The photocatalytic reaction was performed according to the following steps: (i) Air flow in by-pass mode, to obtain a zero reference point; (ii) Incorporation of the pollutant to the total gas flow and stabilization of the trichloroethylene signal in by-pass mode; (iii) Flow of the total gas containing the pollutant through the photocatalytic reactor where the sample was placed in dark conditions, until stabilization of the inlet trichloroethylene signal; and (iv) UV-A irradiation of the sample and evaluation of the photocatalytic activity. The amount of C_2HCl_3 adsorbed by the materials at dynamic conditions was estimated at stage (iii), considering the total gas flow (500 mL min^{-1}) and the concentration of the pollutant at the inlet [C_2CHCl_3] = 25 ppm).

3. Results and discussion

3.1. Preparation of silicalite-1 and TiO_2/silicalite-1 hybrids

Silicalite-1 was prepared at 90 °C in the form of milky suspensions. Fig. 1 shows SEM images of the silicalite-1 samples prepared with GEO40™ SOL-1030Na (a, b) and with Ludox SM (c, d). Silicalite-1 of similar morphology and crystallite size was obtained independently of the colloidal silica type used in the syntheses. GS1N and LS1N samples were composed of spherical particles with a relatively broad particle size distribution and crystal sizes of about 250 nm (Fig. 1a and c). Reducing the amount of TPAOH and diluting the synthesis solution resulted in an increase of the silicalite-1 crystal size and a formation of well-defined crystals exhibiting the typical MFI-type zeolite coffin-shape morphology (Fig. 1, b and d) in accordance to previous results [24]. Another observation is that the surface roughness of GS1N appears higher compared to LS1N, which is more clearly seen from corresponding TEM images (Fig. S1, Supplementary data). The fully crystalline nature of the silicalite-1 samples prepared was further confirmed by HRTEM. In all cases, the particles gave rise to electron diffraction patterns corresponding to the orthorhombic crystal structure of silicalite-1.

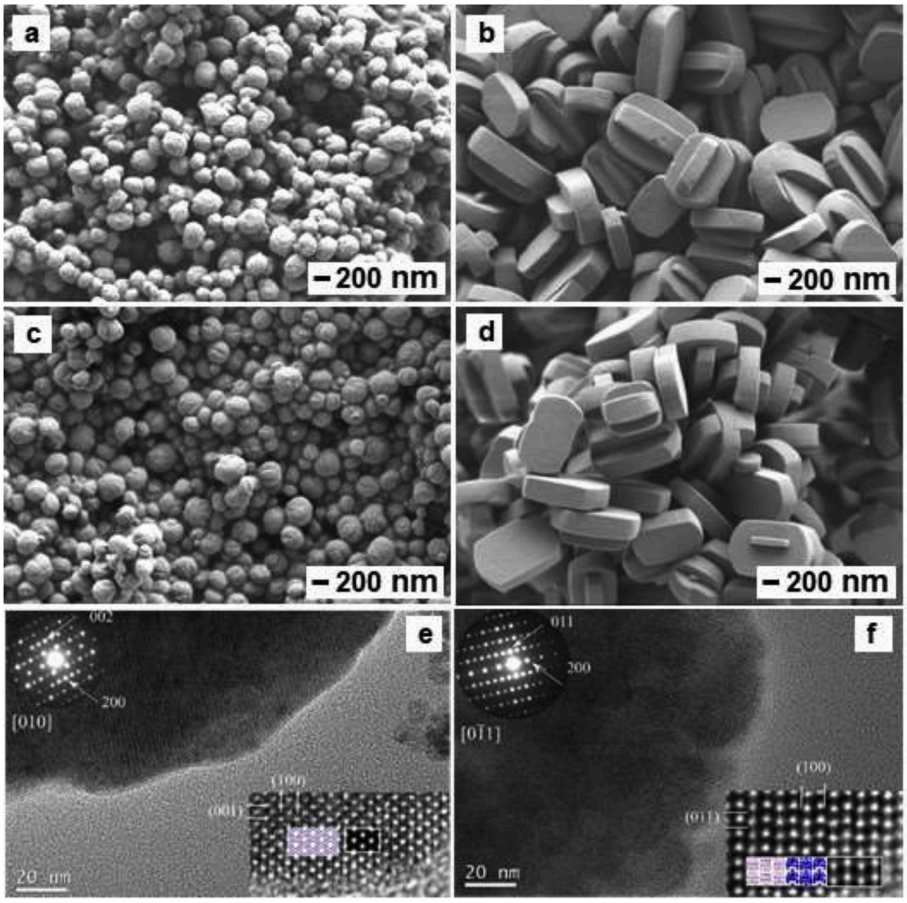

Fig. 1. SEM images of: (a) GS1N, (b) GS1M, (c) LS1N and (d) LS1M. Fig. 1e and f shows high resolution TEM images of GS1N along with the corresponding electron diffraction patterns. Insets: magnified areas of the corresponding images; atomic structure representation is overlaid together with the simulated images.

Furthermore, the reciprocal lattice is composed of well-defined and sharp reflections, which, along with the absence of satellite reflections and diffuse diffracted intensity, indicate that all samples are fully crystalline. As an example, high resolution images and corresponding diffraction patterns of the GS1N sample are presented in Fig. 1e and f. In the insets, the projected atomic structure of silicalite-1 is overlaid to demonstrate the correspondence between the pores in the structure and the contrast in the image. The distribution of pores in the silicalite-1 structure is clearly identified.

The size and the particles size distribution of the silicalite-1 samples prepared were studied by DLS. DLS graphs for S1N samples displayed similar particle size distributions (Fig. 2). The Z-average size was 246 nm for GS1N and 278 nm for LS1N with a polydispersity index (PDI) of 0.091 and 0.080, respectively. The PDI values indicated that both samples were monodispersed. The Z-average sizes determined for GS1M and LS1M were 880 nm (PDI = 0.243) and 844 nm (PDI = 0.231), however, these samples were polydispersed and did not meet data quality for DLS analysis. SEM and DLS results indicated that, as expected, the silica sol precursor used had no influence on the morphology of the resulting samples.

Nitrogen adsorption-desorption measurements were performed to determine the textural characteristics of the silicalite-1 samples prepared. The nitrogen adsorption-desorption isotherms for all samples were type I isotherms typical of microporous materials with an initial steep increase in the volume of gas adsorbed followed by a plateau (Fig. 3). A type H3 hysteresis was also observed in all isotherms, which can be associated with the presence of interparticle mesoporosity in aggregated particles [37,38]. The hysteresis loops were more pronounced for the S1N samples and their pore-size distributions indicated a well-defined broad peak at ca. 40–50 nm. This could be related to the spherical morphology of the samples. The nitrogen adsorption-desorption data further confirm that silicalite-1 synthesized with geothermal silica follows identical crystallization to silicalite-1 formed from Ludox. The results indicate that waste silica recovered from exhaust geothermal fluids can be used as a silica source to prepare silicalite-1, which has very similar textural properties, morphology and crystallinity to silicalite-1 prepared using conventional silica sources.

The silicalite-1 samples prepared using geothermal and Ludox colloidal silica were used to prepare TiO_2/silicalite-1 hybrid samples. The hybrid materials were then tested for the degradation of a model volatile organic compound (VOC), trichloroethylene. No additional peaks due to the presence of TiO_2 were detected in the XRD patterns of the hybrid samples in accordance with our previous results (Fig. S2, Supplementary data) [12]. This indicated that the TiO_2 was well dispersed onto the zeolite crystals with no presence of large TiO_2 aggregates. The morphology and the size of the silicalite-1 samples was not affected during the TiO_2 modification process. TEM images confirmed this conclusion (Fig. 4). The surface of all silicalite-1 samples was coated with TiO_2 crystallites (Fig. 4 and Figs. S3 and S4, Supplementary data). This could explain the substantial increase in the external surface areas of the hybrid samples compared to the surface areas of corresponding silicalite-1 samples (Table 1.) Raman analysis showed that TiO_2 was present in the form of TiO_2-anatase in all hybrid samples (Fig. S5, Supplementary data) [38]. The surface areas of the silicalite-1 samples and the TiO_2/silicalite-1 hybrids were similar (Table 1). However, the impregnation of TiO_2 resulted in a decrease of up to 50% of the micropore volume of the hybrid samples compared to the pure silicalite-1 samples. The silicalite-1 samples showed large C_2HCl_3 adsorption ability with values between 600–700 μmol g^{-1}, similar to that observed for a commercial ZSM-5 zeolite (600 μmol g^{-1}). S1N particles showed higher C_2HCl_3 adsorption ability compared to S1M silicalite-1, related to their higher surface area and micropore volume. The incorporation of TiO_2 reduced the VOC adsorption ability by up to 15% due to the dilution of the zeolite phase and possibly due to pore blocking as observed for other composites. In the case of S1M materials, the incorporation of titania resulted in a slight increase of the surface area, that could be related to a better dispersion of the semiconductor on the silicalite-1 surface. Generally, the higher the micropore volume, the higher the amount of adsorbed organochloride compound, and this amount was significantly higher compared to the amount adsorbed by the TiO_2 xerogel.

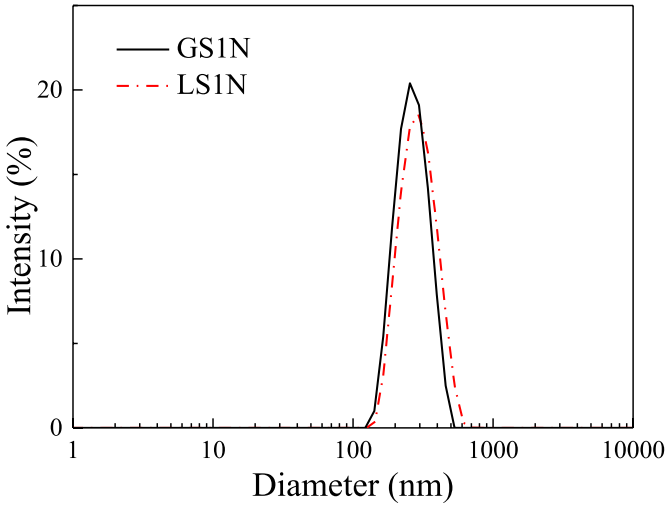

Fig. 2. DLS particle size distributions of GS1N and LS1N.

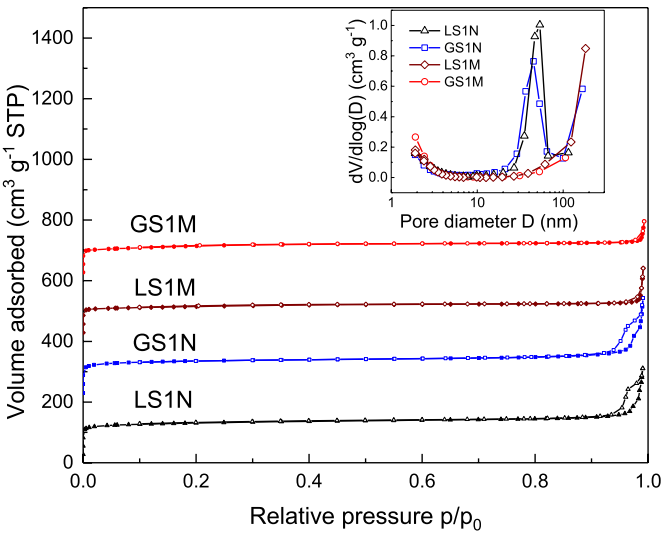

Fig. 3. Nitrogen adsorption-desorption isotherms at 196 °C of the different silicalite-1 samples. For clarity, the isotherms are shifted upwards by 200. The insert shows BJH desorption pore-size distributions.

3.2. Photocatalytic properties

The photocatalytic performance of the TiO_2/silicalite hybrids in the C_2HCl_3 photodegradation was studied at different total gas flows ranging from 500 to 900 mL min^{-1}. The results at 500 mL min^{-1} are shown in Fig. 5. A comparison between the C_2HCl_3 conversion and CO_2 or $COCl_2$ selectivity values for bare TiO_2 and hybrid samples, are shown in Fig. 5a. Other products such as HCl, CO, or dichloroacetylchloride, were observed as minor reaction products [39]. C_2HCl_3 conversion values near 80% were attained for samples hybridized by the microporous materials and the pure TiO_2. However, it has to be taken into account that TiO_2 based composites contain only 8 wt% TiO_2. The main differences between the samples arise when the selectivity to $COCl_2$ and CO_2 is compared. TiO_2/silicalite-1 samples showed around 15% lower $COCl_2$ selectivity compared to bare TiO_2. Moreover all hybrids

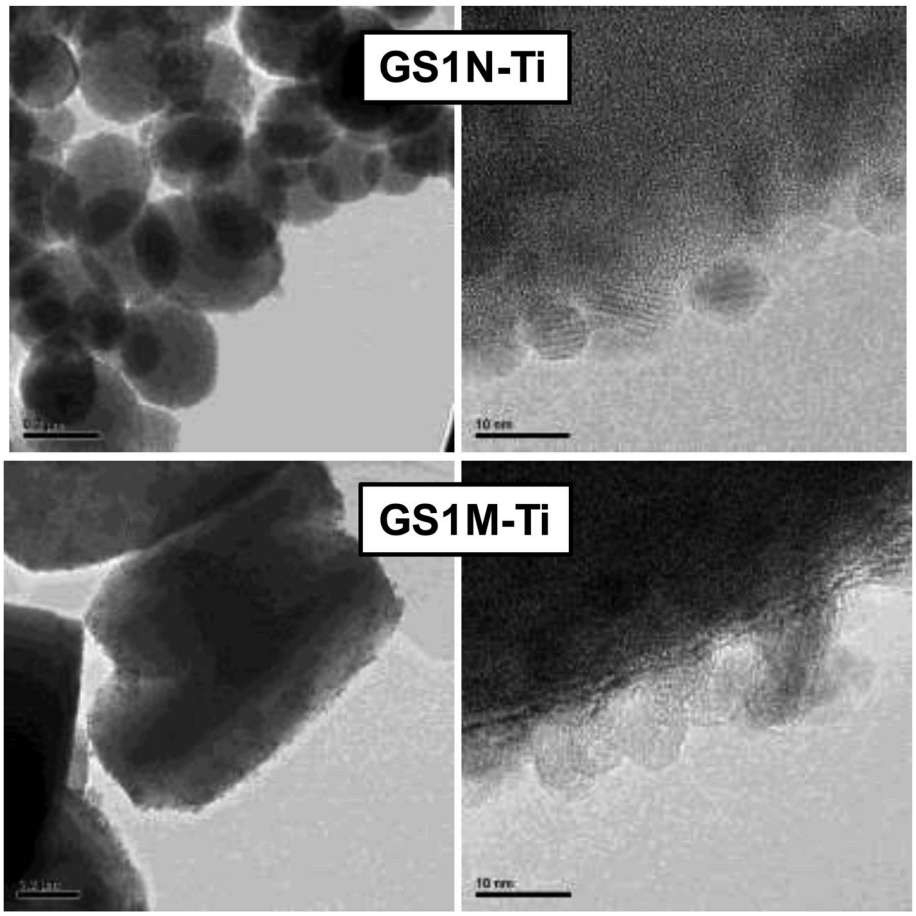

Fig. 4. TEM images of TiO_2/silicalite-1 hybrids.

Table 1
Surface areas (S_{BET}), micropore volumes (V_μ), external surface areas (S_{EXT}) and amount of trichloroethylene adsorbed at 25 °C of silicalite-1 and TiO_2/silicalite-1 hybrid samples. The results for TiO_2-Xg is also included for comparison.

Sample	S_{BET} ($m^2\ g^{-1}$)	V_μ ($cm^3\ g^{-1}$)	S_{EXT} ($m^2\ g^{-1}$)	C_2HCl_3 adsorption (μmol g^{-1} catalyst)
LS1N	428	0.16	89	706
LS1M	375	0.14	78	658
GS1N	441	0.17	84	621
GS1M	377	0.12	126	595
LS1N-Ti	396	0.11	177	600
LS1M-Ti	409	0.07	263	583
GS1N-Ti	397	0.07	252	585
GS1M-Ti	381	0.06	250	531
TiO_2-Xg	149	–	n.d.	203

n.d. – not determined.

independently of the silicalite-1 source, showed higher CO_2 selectivity than TiO_2, thus improving the mineralization process. According to our previous results for hybrids based on ZSM-5 of different SiO_2/Al_2O_3 ratio, an increase of the silica content reduces the formation of $COCl_2$ [12]. This effect was related to the hydrophobic nature of the zeolitic material and the adsorption ability towards the contaminant [40,41]. The results obtained in this work with TiO_2/silicalite-1 samples confirm this hypothesis. TiO_2/silicalite-1 showed between 5 and 10% lower $COCl_2$ selectivity comparing to TiO_2/ZSM-5 [12]. With regards to CO_2, GS1M-Ti showed the highest CO_2 selectivity value above 40%, nearly 8% higher compared to ZSM-5/TiO_2 previously reported [12], and nearly 15% higher compared to that for pure TiO_2. Moreover, it should be highlighted the important role of the silicalite-1 particle size for the final photocatalytic properties. These trends can be better appreciated if the C_2HCl_3 degradation rate and CO_2 and $COCl_2$ formation rate per gram of TiO_2 are represented (Fig. 5b). The higher photocatalytic performance of TiO_2/silicalite-1 compared to bare TiO_2 is clearly observed from this figure. The samples synthesized with Geosol (GS1N-Ti and GS1M-Ti) showed slightly better photocatalytic performance than the ones based on Ludox, which could be due to presence of impurities in the former, for instance Ca and K as specified by the manufacturer (Ca, $\leq$ 500 ppm; K, $\leq$ 900 ppm). Higher traces of Ca and K were detected in the samples prepared from Geosol according to XRF analysis (data not shown). We have observed similar higher catalytic activity for methane oxidation of Pd-loaded FAU zeolites for zeolites prepared with geothermal silica compared to Ludox in our previous study [42]. It is important to point out the high CO_2 formation rate obtained for TiO_2/silicalite-1 synthetized by Geosol compared to the ones prepared by Ludox, particularly for the GS1M-Ti sample. The ability towards the C_2HCl_3 adsorption of this sample is the lowest (Table 1). A moderate adsorption capacity of the pollutant is required in order to promote the photocatalytic activity [40,41]. The photocatalytic process involved adsorption of the contaminant onto the silicalite-1 and a further migration to the TiO_2 active sites, where the photocatalytic process occurs. For this process, it is essential to have an optimum TiO_2 distribution on the high surface area material. C_2HCl_3 conversion values around 60% were obtained by increasing the total gas flow to 900 mL min^{-1}, indicating the good performance of this material for the treatment of high gas volumes.

The C_2HCl_3 photoreduction is a complex process, with many reactions involved. The main reaction goes through Eq. (1), where C_2HCl_3 is photooxidized to CO_2. Nevertheless, other reaction products are produced, such as dichloroacetyl chloride (DCAC) and $COCl_2$ (Eq. (2)

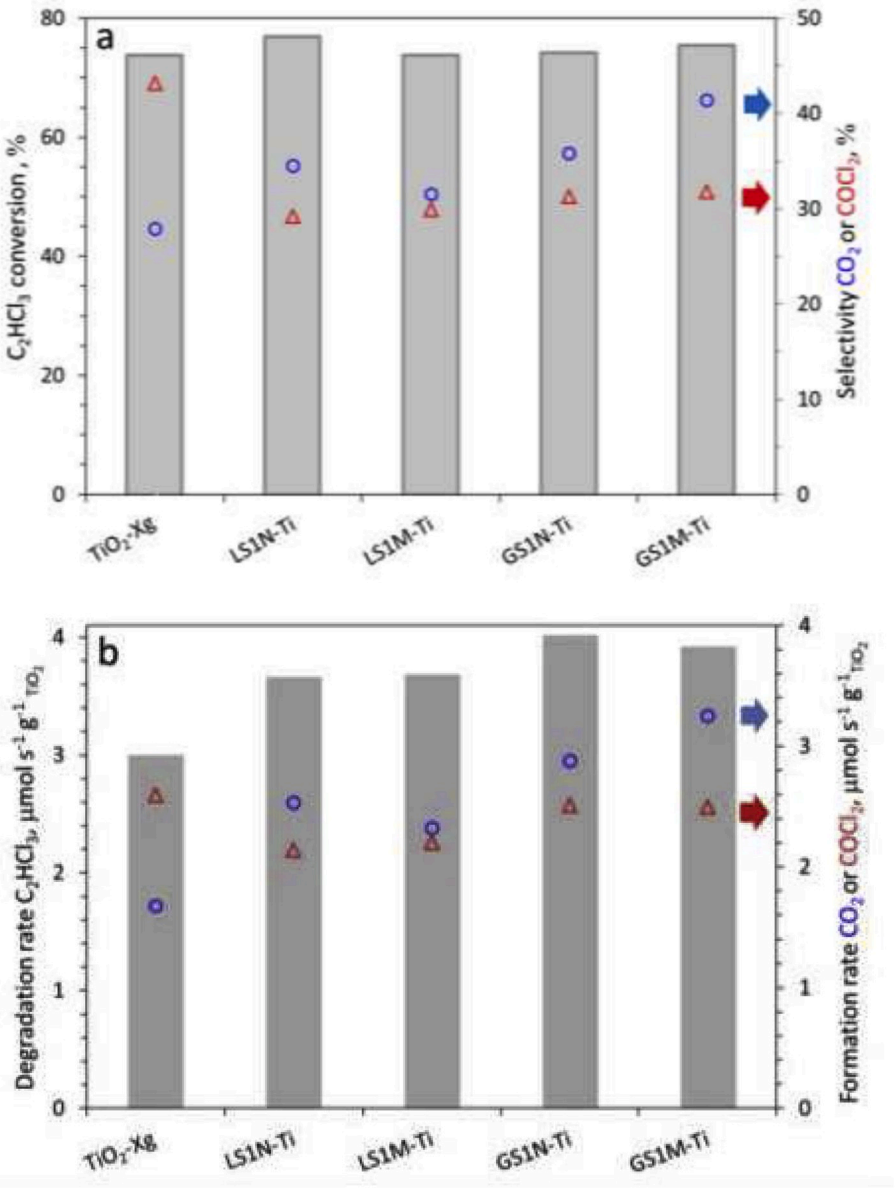

Fig. 5. Photocatalytic activity results for TiO_2/silicalite-1 hybrids and reference TiO_2: a) C_2HCl_3 conversion and CO_2 or $COCl_2$ selectivity values and b) C_2HCl_3 degradation rate and CO_2 and $COCl_2$ formation rates; o - CO_2, Δ - $COCl_2$. Operating conditions: total gas flow F = 500 mL min^{-1}, [C_2HCl_3] = 25 ppm, *tr* = 0.77 s.

and Eq. (3)). Different species may be involved in the reaction such us •OH, O_2* or •Cl [43–45].

$$C_2HCl_3 + {}^3\!/_2 O_2 + H_2O \xrightarrow{hv,\ TiO_2} 2CO_2 + 3HCl \quad (1)$$

$$C_2HCl_3 + {}^1\!/_2 O_2 \xrightarrow{hv,\ TiO_2} Cl_2HCCOCl \quad (2)$$

$$Cl_2HCCOCl + {}^1\!/_2 O_2 \xrightarrow{hv,\ TiO_2} COCl_2 + HCl + CO \quad (3)$$

$$COCl_2 + H_2O \rightarrow CO_2 + HCl \quad (4)$$

Longer residence time or the presence of water vapor on the stream may lead to hydrolysis reaction even in the dark improving the mineralization process (Eq. (4)) [46]. In fact, the experiments were performed in the absence of water vapor on the stream to study the effect of the silicalite-1 nature on the mineralization process. The results suggest that the nature of the silicate-1 has an effect on the adsorption of the reaction intermediates and further oxidation and release to CO_2 into the gas phase. GSM1-Ti was the sample with the lowest $COCl_2$ formation rate. Interestingly, TEM analysis indicated the presence of channels in the GS1N-Ti sample, which were not observed in the other hybrid samples (Fig. 6), which could explain the higher surface roughness, surface area and pore volume values of this material. Moreover, the presence of these channels should be taken into account to explain the photocatalytic performance of this composite. However, understanding the mechanism of formation of these channels was beyond the objectives of the present study and will be analyzed in a future work.

The GS1-Ti samples were further studied by electrophoretic migration measurements. The variation of the zeta potential with pH for silicalite-1 and TiO_2/silicalite-1 samples prepared with geothermal silica are shown in Fig. 7. The silicalite-1 samples showed an isoelectric point (IEP) of 1.6 and <1 for GS1M and GS1N, respectively. The TiO_2 xerogel showed an IEP of around 5. The molar fraction of TiO_2 covering the surface was estimated using the Park's equation. Values of ca. 65% and 50% for GS1M-Ti and GS1N-Ti, respectively, were obtained. The higher fraction of TiO_2 on the GS1M-Ti sample could explain the higher photocatalytic performance of this material compared to GS1N-Ti.

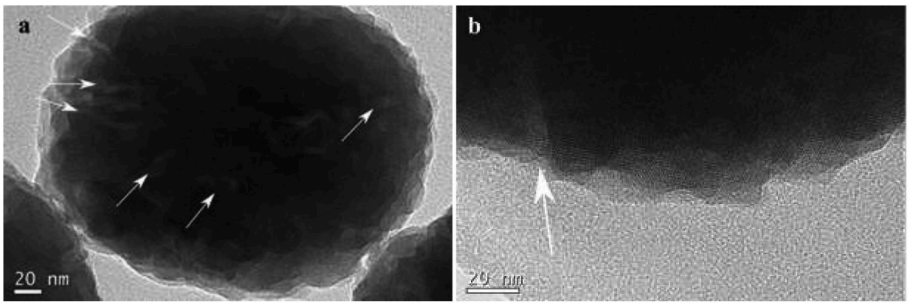

Fig. 6. TEM images of the GS1N-Ti sample. The arrows indicate the presence of pores as evident by the peculiar contrast in the images.

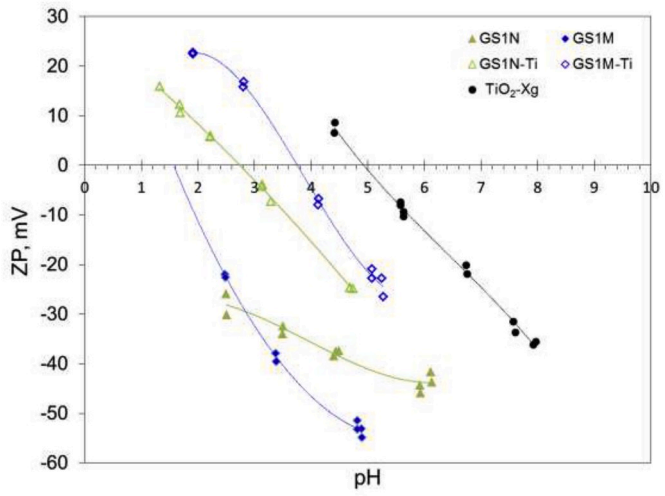

Fig. 7. Zeta potential curves for raw materials and GS1-Ti samples.

4. Conclusion

Submicrometer-sized silicalite-1 samples were prepared using two types of colloidal silica sols, Ludox SM and a silica sol recovered from geothermal fluids, GEO40™ SOL-1030Na. The silicalite-1 samples prepared from the two silica sources showed similar characteristics independently of the synthesis solution used. This shows that geothermal silica sols can be successfully used for synthesis of zeolites. Two silicalite-1 samples were prepared with each silica sol with sizes of about 250 nm (S1N) and 900 nm (S1M), respectively. The former had spherical morphology, whereas larger crystals characterized by typical coffin-shape silicalite-1 crystal morphology. TiO_2/silicalite-1 hybrids were prepared with the two silicate-1 samples. The hybrids were tested as photocatalysts for air purification under UV-A irradiation using C_2HCl_3 as a model VOC molecule. Silicalite-1 improved the adsorption ability of the composite towards the model molecule compared to ZSM-5 used in previous studies as a result of the increased hydrophobicity of silicalite-1. More significantly, the hybrids developed increased the CO_2 selectivity facilitating the VOC mineralization and reduced the formation rates of reaction by-products.

Notes

The authors declare no competing financial interest.

Declaration of competing interests

The authors declare that they have no known competing financial interests or personal relationships that could have appeared to influence the work reported in this paper.

CRediT authorship contribution statement

Silvia Suárez: Conceptualization, Methodology, Investigation, Validation, Writing - original draft, Writing - review & editing, Visualization. **Roxana Postolache:** Investigation. **F. Javier García-García:** Investigation, Writing - original draft, Formal analysis. **Benigno Sánchez:** Resources, Writing - review & editing. **Roger Rothon:** Resources. **Aidan M. Doyle:** Writing - review & editing. **Lubomira Tosheva:** Conceptualization, Methodology, Validation, Supervision, Writing - original draft, Writing - review & editing, Visualization.

Appendix A. Supplementary data

Supplementary data to this article can be found online at https://doi.org/10.1016/j.micromeso.2020.110202.

References

[1] X. Chen, S.S. Mao, Chem. Rev. 107 (2007) 2891–2959.
[2] J. Schneider, M. Matsuoka, M. Takeuchi, J. Zhang, Y. Horiuchi, M. Anpo, D. W. Bahnemann, Chem. Rev. 114 (2014) 9919–9986.
[3] M.D. Hernandez-Alonso, F. Fresno, S. Suarez, J.M. Coronado, Energy Environ. Sci. 2 (2009) 1231–1257.
[4] H. Mamaghani, F. Haghighat, C.-S. Lee, Appl. Catal., B 203 (2017) 247–269.
[5] Y. Boyjoo, H. Sun, J. Liu, V.K. Pareek, S. Wang, Chem. Eng. J. 310 (2017) 537–559.
[6] F. Fresno, R. Portela, S. Suarez, J.M. Coronado, J. Mater. Chem. 2 (2014) 2863–2884.
[7] S. MiarAlipour, D. Friedmann, S. Scott, R. Amal, J. Hazard Mater. 341 (2018) 404–423.
[8] W. Zhang, K. Wang, Y. Yu, H. He, Chem. Eng. J. 163 (2010) 62–67.
[9] W. Zhang, F. Bi, Y. Yu, H. He, J. Mol. Catal. 372 (2013) 6–12.
[10] J. Jansson, S. Suárez, F.J. García-García, B. Sánchez, Top. Catal. 60 (2017) 1171–1182.
[11] H. Yahiro, T. Miyamoto, N. Watanabe, H. Yamaura, Catal. Today 120 (2007) 158–162.
[12] J. Jansson, S. Suárez, F. Javier García-García, B. Sánchez, Appl. Catal., B 178 (2015) 100–107.
[13] S. Gomez, C.L. Marchena, M.S. Renzini, L. Pizzio, L. Pierella, Appl. Catal., B 162 (2015) 167–173.
[14] M. Mahalakshmi, S. Vishnu Priya, B. Arabindoo, M. Palanichamy, V. Murugesan, J. Hazard Mater. 161 (2009) 336–343.
[15] Y. Kuwahara, J. Aoyama, K. Miyakubo, T. Eguchi, T. Kamegawa, K. Mori, H. Yamashita, J. Catal. 285 (2012) 223–234.
[16] K. Guesh, Á. Mayoral, C. Márquez-Álvarez, Y. Chebude, I. Diaz, Microporous Mesoporous Mater. 225 (2016) 88–97.
[17] K. Guesh, Á. Mayoral, Y. Chebude, M.J. López-Muñoz, C. Márquez-Álvarez, I. Diaz, New J. Chem. 42 (2018) 12001–12007.
[18] F. Li, Y. Jiang, L. Yu, Z. Yang, T. Hou, S. Sun, Appl. Surf. Sci. 252 (2005) 1410–1416.
[19] X. Liu, Y. Liu, S. Lu, W. Guo, B. Xi, Chem. Eng. J. 350 (2018) 131–147.
[20] Y. Nomura, S. Fukahori, H. Fukada, T. Fujiware, J. Hazard Mater. 340 (2017) 427–434.
[21] S. Liu, M. Lim, R. Amal, Chem. Eng. Sci. 105 (2014) 46–52.
[22] K. Yamaguchi, K. Inumaru, Y. Oumi, T. Sano, S. Yamanaka, Microporous Mesoporous Mater. 17 (2009) 350–355.
[23] L. Tosheva, V.P. Valtchev, Chem. Mater. 17 (2005) 2494–2513.
[24] A.E. Persson, B.J. Schoeman, J. Sterte, J.-E. Otterstedt, Zeolites 14 (1994) 557–567.
[25] G. Majano, A. Darwiche, S. Mintova, V. Valtchev, Ind. Eng. Chem. Res. 48 (2009) 7084–7091.
[26] Q. Li, B. Mihailova, D. Creaser, J. Sterte, Microporous Mesoporous Mater. 40 (2000) 53–62.
[27] S. Mintova, V. Valtchev, Microporous Mesoporous Mater. 55 (2002) 171–179.

[28] T. Butt, L. Tosheva, Microporous Mesoporous Mater. 187 (2014) 71–76.
[29] Q. Zhang, G. Chen, Y. Wang, M. Chen, G. Guo, J. Shi, J. Luo, J. Yu, Chem. Mater. 30 (2018) 2750–2758.
[30] P. Pengthamkeerati, W. Kraewong, L. Meesuk, Environ. Prog. Sustain. 34 (2015) 188–193.
[31] G.T.M. Kadja, V.A. Fabiani, M.H. Aziz, A.T.N. Fajar, A. Prasetyo, V. Suendo, E.-P. Ng, R. Mukti, Adv. Powder Technol. 28 (2017) 443–452.
[32] M. Finster, C. Clark, J. Schroeder, L. Martino, Renew. Sustain. Energy Rev. 50 (2015) 952–966.
[33] W.A. Chiu, J. Jinot, C.S. Scott, S.L. Makris, G.S. Cooper, R.C. Dzubow, A.S. Bale, M. V. Evans, K.Z. Guyton, N. Keshava, J.C. Lipscomb, S. Barone Jr., J.F. Fox, M. R. Gwinn, J. Schaum, J.C. Caldwell, Environ. Health Perspect. 1213 (2013) 303–311.
[34] M.A. Anderson, M.J. Gieselmann, Q. Xu, J. Membr. Sci. 39 (1988) 243–258.
[35] M.V. Smoluchowski, Ann. Phys. 326 (1906) 756–780.
[36] F.J. Gil-Llambias, A.M. Escudey-Castro, J. Chem. Soc., Chem. Commun. (1982) 478–479.
[37] K.S.W. Sing, D.H. Everett, R.A.W. Haul, L. Moscou, R.A. Pierotti, J. Rouquerol, T. Siemieniewska, Pure Appl. Chem. 57 (1985) 603–619.
[38] L. Tosheva, B. Mihailova, M.A. Wilson, M.A. Carter, J. Eur. Ceram. Soc. 20 (2010) 1867–1872.
[39] M.D. Driessen, T.M. Miller, V.H. Grassian, J. Mol. Catal. 131 (1998) 149–156.
[40] S. Suárez, J.M. Coronado, R. Portela, J.C. Martín, M. Yates, P. Ávila, B. Sánchez, Environ. Sci. Technol. 42 (2008) 5892–5896.
[41] J. Jansson, K. Kobayashi, H. Hori, B. Sánchez, B. Ohtani, S. Suárez, Catal. Today 287 (2017) 22–29.
[42] A.M. Doyle, R. Postolache, D. Shaw, R. Rothon, L. Tosheva, Microporous Mesoporous Mater. 285 (2019) 56–60.
[43] M.A. Anderson, S. Yamazaki-Nishida, S. Cervera-March, D.F. Ollis, H. Al-Ekabi (Eds.), Photocatalytic Purification and Treatment of Water and Air, Elsevier, Amsterdam, 1993, pp. 405–420.
[44] J. Fan, J.T. Yates, J. Am. Chem. Soc. 118 (1996) 4686–4692.
[45] W.A. Jacoby, D.M. Blake, R.D. Noble, C.A. Koval, J. Catal. 157 (1995) 87–96.
[46] W.A. Jacoby, M.R. Nimlos, D.M. Blake, R.D. Noble, C.A. Koval, Environ. Sci. Technol. 28 (1994) 1661–1668.